

# Description of Exotic Nuclei Using Continuum Shell Model

N. Michel<sup>†</sup>, J. Okołowicz<sup>†‡</sup> and M. Płoszajczak<sup>†</sup>

<sup>†</sup> Grand Accélérateur National d'Ions Lourds, CEA/DSM – CNRS/IN2P3, BP 55027, F-14076 Caen Cedex 05, France

<sup>‡</sup> Institute of Nuclear Physics, Radzikowskiego 152, PL - 31342 Krakow, Poland

(today)

In weakly bound exotic nuclei, number of excited bound states or narrow resonances is small and, moreover, they couple strongly to the particle continuum. Hence, these systems should be described in the quantum open system formalism which does not artificially separate the subspaces of (quasi-) bound and scattering states. The Shell Model Embedded in the Continuum provides a novel approach which solves this problem. Examples of application in *sd* shell nuclei will be presented.

21.60.Cs, 23.40.-s, 23.40.Hc, 25.40.Lw

## I. INTRODUCTION

A realistic account of the low-lying states properties in exotic nuclei requires taking into account the coupling between discrete and continuum states. This aspect is particularly important in studies near the drip line where one has to use both structure and reaction data to understand basic properties of these nuclei. Within the Shell Model Embedded in the Continuum (SMEC) [1], one may obtain a unified description of the divergent characteristics, such as the spectra (energies of states, transition probabilities, proton/neutron emission widths,  $\beta$ -decays, etc.) and the reactions involving one-nucleon in the continuum (proton/neutron capture processes, Coulomb dissociation reactions, elastic/inelastic proton/neutron reactions, etc.). The accumulation of divergent observables analyzed in the same theoretical framework provides a stringent test of the effective interactions and permits to assess the mutual complementarity of reaction and structure data for the understanding of exotic configurations and decays in those weakly bound nuclei.

In the SMEC formalism, the subspaces of (quasi-) bound (the  $Q$  subspace) and scattering (the  $P$  subspace) states are separated using the projection operator technique [2].  $P$  subspace contains asymptotic channels, made of  $(N-1)$ -particle localized states and one nucleon in the scattering state.  $Q$  subspace contains many-body localized states which are build up by both the bound state single-particle (s.p.) wave functions and the s.p. resonance wave functions. The wave functions in  $Q$  and  $P$  are properly renormalized in order to ensure the orthogonality of wave functions in both subspaces. The details of the approach can be found in [1,3].

The salient feature of SMEC is that the (quasi-) bound many-body states in  $Q$  are given by the multiconfigurational Shell Model (SM) with the realistic effective interaction, providing the internal mixing of configurations. The coupling between bound and scattering states is described by the density dependent interaction (DDSM1) [3,4]. This interaction provides an external mixing of configurations via the virtual excitations of particles to the

continuum states. A subtle balance of external and internal configuration mixing explains energies and widths of levels,  $(p, p')$  excitation functions, radiative capture processes, etc..

To generate radial s.p. wave functions in  $Q$  and the scattering wave functions in  $P$ , as a first guess, we use the potential of Woods-Saxon (WS) type with the spin-orbit :  $V_{SO}\lambda_\pi^2(2\mathbf{l}\cdot\mathbf{s})r^{-1}df(r)/dr$ , and Coulomb parts included.  $\lambda_\pi^2 = 2\text{fm}^2$  is the pion Compton wavelength and  $f(r)$  is the spherically symmetrical WS formfactor. The Coulomb potential  $V_C$  is calculated for a uniformly charged sphere. This 'first guess' potential  $U(r)$ , is then self-consistently modified by the residual interaction. The iterative procedure yields the self-consistent potential  $U^{(sc)}(r)$ , which depends on channel angular momentum and differs significantly from the initial potential in the interior of the potential well. For weakly bound configurations, also the surface properties of initial potential are changed by the residual coupling. As a result of this self-consistent coupling, the initial SM Hamiltonian in  $Q$  becomes energy dependent and its eigenvalues become complex for decaying many-body states.

## II. THE FIRST-FORBIDDEN MIRROR $\beta$ DECAYS IN A=17 NUCLEI

First-forbidden  $\beta^+$  decay rate ( $f^+$ ) from the ground state (g.s.)  $J^\pi = 1/2_1^-$  of  $^{17}\text{Ne}$  to the weakly bound state  $J^\pi = 1/2_1^+$  in  $^{17}\text{F}$  exhibits an abnormal asymmetry with respect to its mirror  $\beta^-$  decay rate ( $f^-$ ) of  $^{17}\text{N}$  into a well bound excited state of  $^{17}\text{O}$  [5]. This asymmetry has been explained either by large asymmetry of radial sizes of  $1s_{1/2}$  s.p. orbits involved in bound states of  $^{17}\text{F}/^{17}\text{O}$  and  $^{17}\text{Ne}/^{17}\text{N}$  [5] or by the charge-dependent effects leading to different amplitudes of  $\pi(0p_{1/2}^2 1s_{1/2}^2)\nu(0p_{1/2}^1)$  and  $\nu(0p_{1/2}^2 1s_{1/2}^2)\pi(0p_{1/2}^1)$  components in the g.s. wave functions of  $^{17}\text{Ne}$  and  $^{17}\text{N}$ , respectively [6]. These two qualitative analysis of the mirror asymmetry lack a consistent treatment of radial properties of the wave functions which are involved in these transitions.

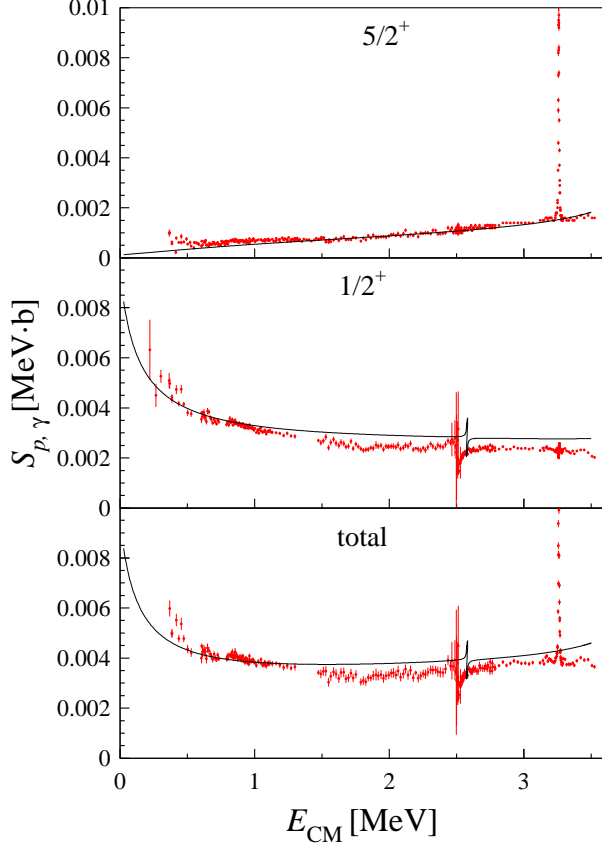


FIG. 1. The astrophysical  $S$ -factor for the reaction  $^{16}\text{O}(p,\gamma)^{17}\text{F}$  leading to the states  $5/2_1^+$  and  $1/2_1^+$  is plotted as a function of the center of mass energy  $E_{CM}$  [4]. The experimental data are from [7]. The diffuseness parameter of the initial WS potential  $U(r)$  is  $a = 0.55$  fm. The depth of  $U(r)$  is chosen in such a way that the self-consistent potential yields the binding energies of proton s.p. orbits  $0d_{5/2}$  and  $1s_{1/2}$  at the experimental binding energies of  $5/2_1^+$  and  $1/2_1^+$  many-body states in  $^{17}\text{F}$  (from [4]).

The stringent constraint on the diffuseness of the mean-field generating radial s.p. wave functions is provided by the proton radiative capture cross section (the astrophysical  $S$ -factor)  $^{16}\text{O}(p,\gamma)^{17}\text{F}$  to the ‘proton halo state’  $1/2_1^+$ , which in the formalism of SMEC can be calculated using not only the same wave functions in  $Q$  and  $P$ , but also the same SM interaction, residual coupling or the initial average potential, as those used in the calculation of the decay rate  $^{17}\text{Ne}(\beta^+)^{17}\text{F}$  and the spectrum of  $^{17}\text{F}$ . Fig. 1 compares measured astrophysical  $S$ -factor for the reaction  $^{16}\text{O}(p,\gamma)^{17}\text{F}$  with the results of the SMEC calculations using ZBM interaction in  $(p_{1/2}d_{5/2}s_{1/2})$  shells. The capture cross-section data can be well reproduced using  $U(r)$  with the surface diffuseness in the range :  $a = 0.55 \pm 0.05$  fm.

Having determined the surface features of the mean-field, we can estimate the charge-dependent effects in  $1s_{1/2} \rightarrow 0p_{1/2}$  dominant contribution to the first-

forbidden mirror  $\beta$  transitions systems. The calculation of the nuclear matrix elements and, hence, the first-forbidden  $\beta$ -decay rates are done using the formalism of Towner and Hardy [8]. Following the analysis of Warburton et al. [9] for  $A \sim 16$ , the matrix element  $\xi'v$  of the time-like piece of the axial current is multiplied by a constant factor 1.61 to account for an enhancement due to meson-exchange currents.

The experimental rate  $f^+$  for  $^{17}\text{Ne}(\beta^+)^{17}\text{F}$  is reproduced by the SMEC calculation with ZBM-F interaction. This hybrid interaction reproduces exactly the experimental energy splitting between the g.s.  $5/2_1^+$  and the first excited state  $1/2_1^+$  in  $^{17}\text{F}$ . However, for the same interaction the measured rate  $f^-$  for  $^{17}\text{N}(\beta^-)^{17}\text{O}$  is over-predicted by a factor  $\sim 3$ . Since the radial dependences which are consistent with the proton capture data give an excellent fit of both the  $\beta^+$  decay rate and the spectrum of  $^{17}\text{F}$ , the discrepancy for  $f^-$  and  $f^+/f^-$  is uniquely due to the deficiency of ZBM-F interaction to reproduce the configuration mixing in  $^{17}\text{O}$  and  $^{17}\text{N}$ , *i.e.* by the charge-dependent effects in the  $Q$  space SM Hamiltonian.

How large are these effects? An essential parameter here is the amplitude of a component  $(1s_{1/2}^2 0p_{1/2}^{-1})$  in the g.s. wave functions of  $^{17}\text{Ne}$  and  $^{17}\text{N}$ . Experimental values for  $f^-$  and  $f^+/f^-$  are reproduced if the amplitude of  $(1s_{1/2}^2 0p_{1/2}^{-1})$  in g.s. of  $^{17}\text{N}$  is reduced by  $\sim 30\%$ . In a simplest way, this can be achieved by reducing the separation of  $0d_{5/2}$  and  $1s_{1/2}$  shells in ZBM-F interaction. This new interaction, called ZBM-O\*, reproduces also well the experimental spacing of  $5/2_1^+$  and  $1/2_1^+$  levels in  $^{17}\text{O}$ . One should notice that this important reduction of the  $(1s_{1/2}^2 0p_{1/2}^{-1})$  amplitude concerns a very small component of the g.s. wave function of  $^{17}\text{Ne}$  and  $^{17}\text{N}$ . The dominant component, which is  $(0d_{5/2}^2 0p_{1/2}^{-1})$ , changes by less than 5% going from ZBM-F interaction to ZBM-O\* interaction. Also the dominant  $1p-0h$  configuration in g.s.  $5/2_1^+$  and first excited  $1/2_1^+$  states of  $^{17}\text{F}$  (ZBM-F) and  $^{17}\text{O}$  (ZBM-O\*) is only slightly modified ( $\sim 12\%$ ). Of course, one should be aware that these estimates of charge-dependent effects in SM Hamiltonian can be somewhat affected by the chosen ZBM valence space. In particular, the absence of  $0p_{3/2}$  and  $0d_{3/2}$  subshells leads to an amplification of the sensitivity in the  $1s_{1/2} \rightarrow 0p_{1/2}$  contribution to the charge-dependent effects [6]. Nevertheless, for the first time the quantitative extraction of charge-dependent effects, separately on the radial properties of wave functions and on the configuration mixing in mirror systems, became possible.

### III. BINDING ENERGIES IN NEUTRON-RICH OXYGEN ISOTOPES

As a second example of application of the SMEC formalism, we shall consider the correction to the SM g.s.

energy due to the continuum coupling. In this section,

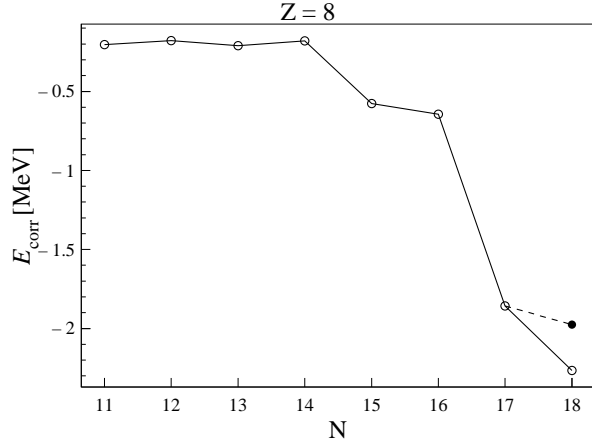


FIG. 2. The SMEC energy correction to the g.s. masses of oxygen isotopes is calculated in the full  $sd$  shell using a Widenenthal effective interaction [10].

we use the valence space of full  $sd$  shell and the effective interaction of Widenenthal [10]. One- and two-neutron separation energies ( $S_n$  and  $S_{2n}$ , respectively) have been calculated for this isotope chain using SM in the same effective space and for the same effective interaction [11]. Fig. 2 shows the above mentioned energy correction  $E_{corr}$  to the SM masses in the chain of neutron-rich isotopes of oxygen.  $E_{corr}$  strongly increases while approaching the neutron drip line. The 'odd-even staggering' reflects a sensitive dependence of this correction on the one-neutron separation energy  $S_n$ , which exhibits a similar dependence. This alone is however not sufficient. The second important effect is related to odd-even variation in the density of many-body states in the  $N-1$  system determining the overall number of channels by which system  $N$  couples to the scattering continuum.

Particularly large coupling matrix elements correspond to the isoscalar couplings between proton and neutron fluids. In the example shown in Fig. 2, these couplings are absent (number of protons in  $sd$  shell equals zero), but one expects that the SMEC energy correction to SM masses will strongly increase when both fluids are present. This may indicate a large shift of the position of the neutron drip line between oxygen and fluor.

SMEC correction to SM masses depends strongly on the radial wave functions in  $Q$ . An example of this kind can be seen in Fig. 2. For oxygen isotopes, the standard isospin dependence of the depth of the central potential yields  $0d_{3/2}$  s.p. state for neutrons unbound for  $N < 18$ . With increasing  $N$ , the energy of  $0d_{3/2}$  resonance is going down and for  $N = 18$  it becomes bound by  $\sim 200$  keV. In view of the uncertainty concerning the isospin dependence of the central potential, we have calculated  $E_{corr}$  for  $^{26}\text{O}$  ( $N = 18$ ) by keeping  $0d_{3/2}$  in the continuum at  $\sim 50$  keV. The full point for  $N = 18$  gives an idea of the sensitivity of  $E_{corr}$  to the asymptotic properties of  $0d_{3/2}$

s.p. state.

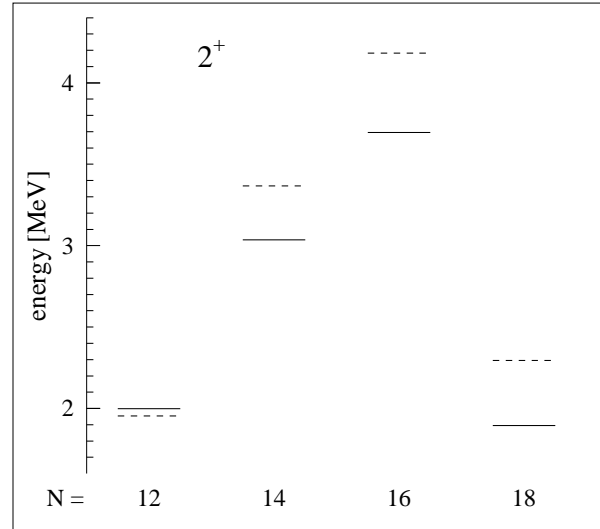


FIG. 3. Excitation energy of  $2^+$  excited state in even- $N$  isotopes of O calculated in SMEC (solid line) and in SM (the dashed line).

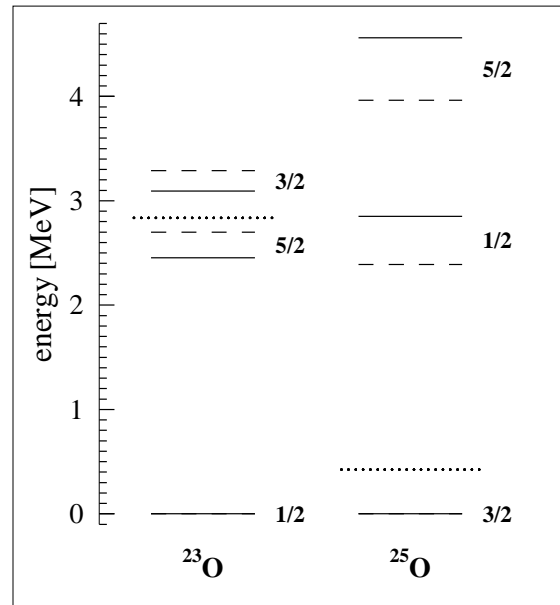


FIG. 4. Lowest energy states in odd- $N$  oxygen isotopes around  $^{24}\text{O}$ . The dotted line shows the position of one-neutron emission threshold. SMEC and SM results are shown with the solid and dashed lines, respectively.

When approaching neutron drip line, the two neutron separation energy  $S_{2n}$  decreases fast and may become smaller than  $S_n$ . In this case, the dominant continuum coupling corresponds to a virtual excitation of nucleon

pairs, which are not yet included in SMEC. For that reason, the SMEC correction close to neutron drip line has to be considered as a lower limit of the continuum influence on SM masses.

Independent information about the configuration dependence of the continuum coupling is provided by the position of the  $2_1^+$  state in even- $N$  oxygen isotopes. In Fig. 3, we compare results of SM and SMEC, which are obtained using the same model space and interaction in  $Q$ . One can see that the relative shift of  $2_1^+$  with respect to the g.s.  $0_1^+$  depends on  $N$ , and in some cases the continuum coupling shifts this state upwards with respect to the SM prediction. However particularly interesting is  $^{24}\text{O}$ , for which the dominant g.s. configuration does not contain the contribution from  $0d_{3/2}$  s.p. resonance, whereas this resonance is strongly populated in  $2_1^+$  state. We can see that the relative shift of  $2_1^+$  state in SMEC calculations for  $^{24}\text{O}$  is particularly strong, reflecting different radial asymptotic properties of the dominant configuration.

A spectacular example of the dependence of the SMEC energy correction on the s.p. radial wave functions in  $Q$  is shown in Fig. 4. Here the lowest energy states of  $^{23}\text{O}$  and  $^{25}\text{O}$  are shown for SMEC (the solid lines) and SM (the dashed lines). Zero of the energy scale corresponds to the g.s. in both cases. G.s. of  $^{23}\text{O}$  does not contain any significant component involving the occupation of the s.p. resonans  $0d_{3/2}$ , and the SMEC correction for excited states  $5/2_1^+$  and  $3/2_1^+$  close to the threshold (the dotted line) are larger than in the g.s. In  $^{25}\text{O}$ , on the contrary,  $0d_{3/2}$  s.p. resonans is strongly occupied in the g.s. and, therefore, excited states  $1/2_1^+$  and  $5/2_1^+$  in SMEC calculations are shifted upwards with respect to their position in the SM.

Not only the absolute energy corrections are large for nuclei near the neutron drip-line, as shown in Fig. 2 for the g.s. of even-even nuclei, but also the relative shifts of excited states with respect to the g.s. can be large and of different signs depending on the radial features of s.p. orbits involved, the internal configuration mixing provided by the SM effective interaction, and the external configuration mixing which depends on the size of the coupling matrix elements for different channels in  $[(N-1)\otimes n]^{J^\pi}$ . Systematic experimental investigation of these salient tendencies of the multiconfigurational continuum shell model remains a challenge for future studies.

#### IV. OUTLOOK

With the SMEC, the new paradigm is born for the microscopic understanding of low-lying properties of unstable nuclei. Fruitful exchanges with the standard SM, which nowadays experience a revival in medium-heavy nuclei and allows to perform no-core calculations till  $^{16}\text{O}$ ,

allows to hope for a new wave of exciting future developments in the field of exotic nuclei.

We wish to thank G. Martínez-Pinedo, T. Otsuka and F. Nowacki for useful discussions.

- 
- [1] K. Bennaceur, F. Nowacki, J. Okołowicz and M. Płoszajczak (1998) *J. Phys.*, **G 24**, 1631; *Nucl. Phys.* **A 651**, 289.
  - [2] H.W. Bartz, I. Rotter, and J. Höhn (1977) *Nucl. Phys.*, **A 275**, 111; *Nucl. Phys.* **A 307**, 285; I. Rotter (1991) *Rep. Prog. Phys.*, **54**, 635.
  - [3] K. Bennaceur, F. Nowacki, J. Okołowicz and M. Płoszajczak (2000) *Nucl. Phys.*, **A 671**, 203.
  - [4] K. Bennaceur, N. Michel, F. Nowacki, J. Okołowicz and M. Płoszajczak (2000) *Phys. Lett.*, **B 488**, 75.
  - [5] M.J.G. Borge et al. (1993) *Phys. Lett.* **B 317**, 25; G. Martínez-Pinedo, PhD thesis, Universidad Autónoma de Madrid.
  - [6] D.J. Millener (1997) *Phys. Rev.*, **C 55**, R1633.
  - [7] R. Morlock et al. (1997) *Phys. Rev. Lett.*, **79**, 3837.
  - [8] I.S. Towner and J.C. Hardy (1972) *Nucl. Phys.*, **A 179**, 489.
  - [9] E.K. Warburton, I.S. Towner and B.A. Brown (1994) *Phys. Rev.*, **C 49**, 824.
  - [10] B.H. Wildenthal (1984) *Prog. Part. Nucl. Phys.*, **11**, 5.
  - [11] E. Caurier, F. Nowacki, A. Poves and J. Retamosa (1998) *Phys. Rev.* **C 58**, 2033.